Analysis and Design of A Robust Class E^2 DC–DC Converter for Megahertz Wireless Power Transfer

Ming Liu, *Student Member, IEEE*, Yue Qiao, Shuangke Liu, *Student Member, IEEE*, and Chengbin Ma, *Member, IEEE*

***Abstract*—Wireless power transfer (WPT) working at megahertz (MHz) is widely considered a promising technology for midrange and low-power applications. A Class E^2 dc–dc converter is composed of a Class *E* power amplifier (PA) and a Class *E* rectifier. It is attractive for applications in MHz WPT due to the soft-switching properties of both the PA and the rectifier. Using the existing design, the Class E^2 dc–dc converter can only achieve optimal performance such as a high efficiency under a fixed operating condition. Meanwhile, in real applications variations in the coil relative position and the final load are common. The purpose of this paper is to analyze and develop a general design methodology for a robust Class E^2 dc–dc converter in MHz WPT applications. Component and system efficiencies are analytically derived, which serve as the basis for the determination of the design parameters. The classical matching network of the Class *E* PA is also improved that provides the required impedance compression capability. Then, a robust parameter design procedure is developed. Both the experimental and calculated results show that proposed design approach can significantly improve the robustness of the efficiency of the Class E^2 dc–dc converter against variations in coil relative position and final load. Finally, the experiments show that the range of variation of the system efficiency is narrowed from 47.5%–85.0% to 73.3%–83.7% using the proposed robust design.**

***Index Terms*—Class E^2 dc–dc converter, efficiency, matching network, robust analysis and design, wireless power transfer (WPT).**

NOMENCLATURE

Z_0	Input impedance of matching network.
Z_{in}	Input impedance of coupling coils.
Z_{rec}	Input impedance of Class *E* rectifier.
C_S	Shunt capacitor of Class *E* power amplifier.
C_0	Series capacitor of matching network.
C_1	Shunt capacitor of matching network.
C_{rx}	Compensation capacitor of receiving coil.
C_r	Parallel capacitor of Class *E* rectifier.
V_{pa}	DC input voltage of Class *E* power amplifier.
P_{in}	Input power of Class *E* power amplifier.
P_o	Output power of Class *E* rectifier.
D	Duty cycle of diode in Class *E* rectifier.
k	Mutual inductance coefficient.
d	Distance between coupling coils.
R_L	Final dc load.

Manuscript received February 8, 2016; revised May 1, 2016; accepted May 16, 2016. Date of publication May 27, 2016; date of current version January 20, 2017. This work was supported by the Shanghai Natural Science Foundation under Grant 16ZR1416300. Recommended for publication by Associate Editor M. Duffy.

M. Liu and S. Liu are with University of Michigan-Shanghai Jiao Tong University Joint Institute, Shanghai Jiao Tong University, Shanghai 200240, China (e-mail: mikeliu@sjtu.edu.cn; liushuangke@sjtu.edu.cn).

C. Ma is with the University of Michigan-Shanghai Jiao Tong University Joint Institute and School of Mechanical Engineering, Shanghai Jiao Tong University, Shanghai 200240, China (e-mail: chbma@sjtu.edu.cn).

Y. Qiao is with GE AVIC Civil Avionics Systems Company Limited, Shanghai 200241, China (e-mail: chimmy@sjtu.edu.cn).

Color versions of one or more of the figures in this paper are available online at http://ieeexplore.ieee.org.

Digital Object Identifier 10.1109/TPEL.2016.2573839

I. INTRODUCTION

In recent years wireless power transfer (WPT) using inductive resonance coupling has become increasingly popular. The technology is now being applied to charge cellphones, wearable devices, and even electric vehicles, etc. [1], [2]. For large-power applications, WPT working at kilohertz (kHz) is making rapid progress particularly in terms of coil design and control [3]–[5]. At the same time, in order to further improve the spatial freedom of WPT, i.e., a longer transfer distance and a higher tolerance to the coil misalignment, it is desirable to increase the operating frequency to several megahertz (MHz) such as 6.78 and 13.56 MHz [2], [6]. Designs with higher operating frequencies result in more compact and lighter WPT systems. However, a major limitation is the insufficient power capability of the present switching devices when working in the MHz frequency band. Therefore, the MHz WPT is usually considered to be suitable for midrange and low-power applications [2], [7]–[9]. This presents a technical challenge because high switching loss occurs when the conventional hard-switching-based power amplifiers (PA) and rectifiers are operated in the MHz range. The soft-switching-based PAs and rectifiers are promising candidates to build high-efficiency MHz WPT systems, such as the Class *E* PA and rectifier.

The Class *E* PA was first introduced for high-frequency applications in [10]. It has been applied in MHz WPT systems thanks to its high efficiency and simple structure [11]–[14]. The Class *E* PA can achieve a very high efficiency when it satisfies zero-voltage switching (ZVS) and zero-voltage-derivative switching (ZVDS) conditions. Similarly, the Class *E* rectifier has also been proposed for high-frequency rectification [15]. Various topologies of the Class *E* rectifier were developed later such as current-/voltage-driven and half-/full-wave ones [16]–[21]. The application of the Class *E* rectifier in WPT was first investigated in [22]. As mentioned previously, a high-efficiency (94.43%) rectifier was reported at an 800-kHz operating frequency. Thus both the Class *E* PA and rectifier can be applied to achieve high-efficiency WPT systems working at MHz, namely the so-called Class E^2 dc–dc converters. A state-space-based analysis of a Class E^2 dc–dc converter is provided for a 200-kHz WPT application in [23]. Initial discussion on the Class E^2 dc–dc converter for MHz WPT can be found in [24]. Meanwhile, as to the knowledge of the authors, studies on a system-level

design of the Class E^2 dc–dc converter for MHz WPT applications are still few. In [25], progress is reported on the optimized design of a 6.78-MHz WPT system, in which both the Class *E* PA and the Class *E* rectifier are used, i.e., a Class E^2 dc–dc converter. The converter is optimized to achieve: 1) ZVS operation of the Class *E* PA, 2) exact resonance of the coupling coils, and 3) a 50% duty cycle of the rectifying diode to lower its voltage stress. However, the limitation of the design is that it can only guarantee optimized performance for a target operating condition, namely fixed coil relative position and final dc load.

In real applications, changes in the coil relative position and final dc load are common. Using the existing design, deviation from its fixed target condition would significantly affect the performance of the system such as the efficiency. In order to improve the robustness of the performance in real applications, it is important to investigate and develop a design methodology that maintains a high performance over a wide range of the operating conditions, i.e., different coil relative position and final dc load. Systematic efforts are required that provide analysis on the component- and system-level efficiencies, possible circuit improvement, and design of system parameters for robustness enhancement (i.e., robust design). The purpose of the proposed robust design is not to exactly achieve the aforementioned three optimal conditions in the existing design, but to determine a solution that improves the system performance over a wide range of operating conditions such as varying coil relative position and final dc load.

Based on the aforementioned basic considerations, this paper develops a systematic and general design methodology for a robust Class E^2 dc–dc converter in MHz WPT applications. It is organized as follows. Section II analytically derives the efficiencies of the Class *E* PA, coupling coils, the Class *E* rectifier, and thus, the efficiency of the overall WPT system. Based on the results of the analytical derivations, the robust analysis and design are performed in Section III. The existing design is shown to have a poor robustness when there are variations in the coil relative position and the final dc load. It is known that a well-designed matching network can achieve better load/power ranges in resonant power converters [26], [27]. The series *LC* circuit was used as the matching network of the Class *E* PA when the PA was first developed in 1975 [10]. In order to improve the robustness of the WPT system, this classical matching network is modified to provide the required impedance compression capability. Then, the robust parameter design procedure is developed. Section IV experimentally validates the previously mentioned robust analysis and design using an example 6.78-MHz WPT system. Finally, Section V draws the conclusion.

II. Derivations of Efficiencies

A Class E^2 dc–dc converter for MHz WPT consists of a Class *E* PA, coupling coils, and a Class *E* rectifier. In this paper, a 6.78-MHz Class E^2 dc–dc converter shown in Fig. 1(a) is used as an example to develop and explain the proposed design methodology, in which series–series coupling coils and a Class *E* current-driven half-wave rectifier are employed. The analytical derivation of the Class *E* current-driven half-wave rectifier has been provided [25]. This helps to simplify the following discussion. In addition, the current-driven rectifier requires a sinusoidal input current, and thus, a receiving series-resonant coil. It is known that there are different topologies for the coupling coils (series–series, parallel–series, series–parallel, and parallel–parallel) and the Class *E* rectifier (current- and voltage-driven, half- and full-wave). The proposed methodology itself is a general one that can be extended to other types of Class E^2 dc–dc converters. For the following discussions, the system and component efficiencies are defined as follows [see Fig. 1(a)]:

$$\eta_{\text{sys}} = \eta_{\text{pa}} \cdot \eta_{\text{coil}} \cdot \eta_{\text{rec}} = \frac{P_o}{P_{\text{in}}} \tag{1}$$

where

$$\eta_{\text{pa}} = \frac{P_{Z_{\text{in}}}}{P_{\text{in}}},\ \eta_{\text{coil}} = \frac{P_{\text{rec}}}{P_{Z_{\text{in}}}},\ \text{and}\ \eta_{\text{rec}} = \frac{P_o}{P_{\text{rec}}}. \tag{2}$$

As shown in Fig. 1(a), P_{in} is the input power of the PA; $P_{Z\text{in}}$ is the input power of the coupling coils; P_{rec} is the input power of the rectifier; and P_o is the output power of the rectifier. Fig. 1(b) and (c) are the equivalent circuit models for following derivations of the efficiencies of the PA and the coupling coils, respectively. In Fig. 1, k and R_L are the two variables that represent mutual inductance coefficient (i.e., coil relative position) and final dc load, respectively, the two major sources of uncertainty in WPT systems. The other parameters are the circuit parameters of the Class *E* PA, coupling coils, and the Class *E* rectifier.

A. Class E PA

As shown in Fig. 1(b), a typical Class *E* PA consists of a dc power supply V_{pa}, an RF (radio frequency) choke L_f, a switch Q, a shunt capacitor C_S, and a matching network. Z_{in} is the input impedance of the coupling coils. Z_0 $(= R_0 + jX_0)$ is the input impedance of the matching network, i.e., the impedance seen by the PA. R_0 and X_0 are jointly determined by the matching network and the impedance Z_{in} (R_0 and X_0 are derived later in Section III-B). Under the condition of a 50% duty cycle of Q, (3)–(7) can be used to derive the efficiency of the PA [28]

$$I_{m,\text{out}} = aI_{\text{pa}} = a\frac{V_{\text{pa}}}{R_{\text{dc}}} \tag{3}$$

$$R_{\text{dc}} = \frac{\pi^2 - a(2\pi\cos\phi - 4\sin\phi)}{4\pi\omega C_S} \tag{4}$$

where

$$a = \frac{2\pi\sin(\varphi+\phi) + 4\cos(\varphi+\phi)}{4\cos\phi\sin(\varphi+\phi) + \pi\cos\varphi} \tag{5}$$

$$\phi = \arctan\frac{\frac{\pi^2}{2} - 4 - \pi\omega C_S(2R_0 + \pi X_0)}{\pi + \pi^2\omega C_S R_0 - 2\pi\omega C_S X_0} \tag{6}$$

$$\varphi = \arctan\frac{X_0}{R_0}. \tag{7}$$

a and φ are the intermediate variables; I_{pa} is the dc input current of PA; $I_{m,\text{out}}$ is the amplitude of i_{out}, the output current of PA; ϕ is initial phase of i_{out}; and R_{dc} is the equivalent resistance PA

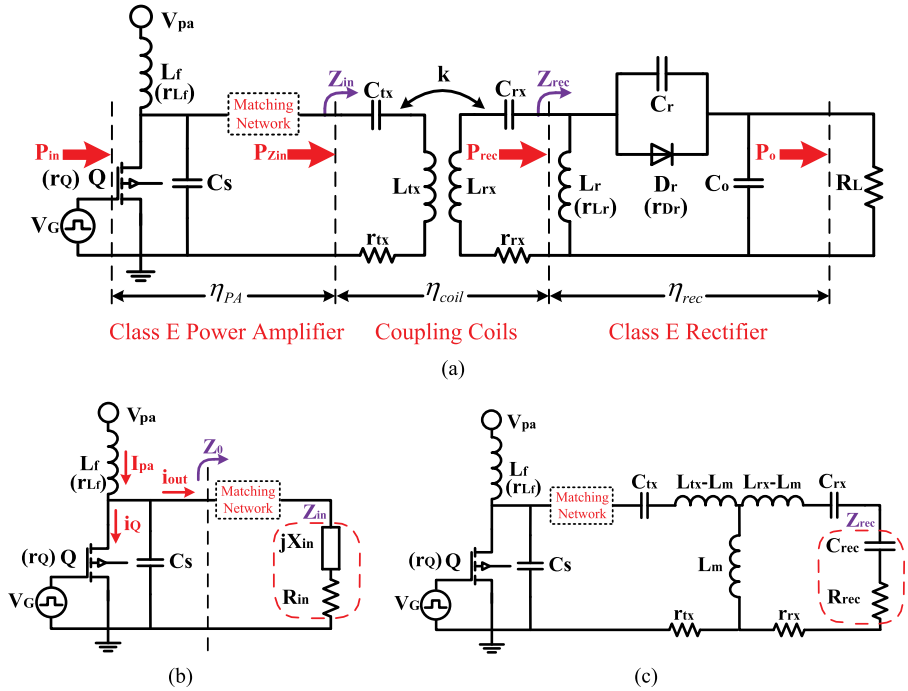

Fig. 1. Class E^2 dc–dc converter for WPT. (a) Circuit model. (b) Equivalent circuit model using Z_{in}. (c) Equivalent circuit model using Z_{rec}.

shows to the dc power supply. According to Fig. 1(b), the current i_Q $(= I_{\text{pa}} - i_{\text{out}})$ flows through the switch when Q is ON. Taking the power losses on switch Q, L_f, and the matching network into consideration, the total input power of the PA, P_{in}, is

$$P_{\text{in}} = P_{R_{\text{dc}}} + P_Q + P_{L_f} + P_{\text{MN}} \tag{8}$$

where $P_{R_{\text{dc}}}$ is input power on the equivalent dc load R_{dc}; P_Q is the conduction loss on the switch Q; P_{MN} is the average power loss on the matching network; and P_{L_f} is the power loss due to r_{L_f}, the equivalent series resistance (ESR) of L_f. In the present MHz WPT system, the gate driving current of the switch and the leakage current during the off-state of switch are small compared with the currents that flow through the switch and the matching network. Thus, the gate driving and off-state power losses are neglected in (8). The power losses can be, respectively, calculated as

$$P_{R_{\text{dc}}} = I_{\text{pa}}^2 R_{\text{dc}},\ P_{L_f} = I_{\text{pa}}^2 r_{L_f},\ \text{and}\ P_{\text{MN}} = \frac{I_{m,\text{out}}^2 r_{L_0}}{2} \tag{9}$$

where r_{L_0} is the ESR of the inductor, L_0, in the matching network (refer to Figs. 2 and 4 in Section III). In this paper, the duty cycle of the Class *E* PA is 50% [13], [29]. Note that in the following discussions, the variation of the duty cycle of the diode in the Class *E* rectifier is limited in order to lower the voltage stress on the rectifying diode. The conduction loss of the switch Q is

$$P_Q = \frac{1}{2\pi}\int_0^{\pi} i_Q^2 r_Q \, d\omega t = \left(\frac{1}{2} + \frac{a}{\pi} + \frac{a^2}{4}\right) I_{pa}^2 r_Q \tag{10}$$

where r_Q is the on-resistance of Q. Since i_{out} is sinusoidal, the output power of the PA, $P_{Z_{\text{in}}}$, is

$$P_{Z_{\text{in}}} = \frac{I_{m,\text{out}}^2 R_0}{2} - P_{\text{MN}} = \frac{a^2 I_{\text{pa}}^2}{2}(R_0 - r_{L_0}). \tag{11}$$

Combining (8)–(11), η_{pa} can be expressed as

$$\eta_{\text{pa}} = \frac{P_{Z_{\text{in}}}}{P_{\text{in}}} = \frac{a^2(R_0 - r_{L_0})}{2R_{dc} + 2r_{L_f} + a^2 r_{L_0} + \left(1 + \frac{2a}{\pi} + \frac{a^2}{2}\right) r_Q}. \tag{12}$$

As shown in aforementioned equations, the PA efficiency relates to the parameters C_S and Z_0 $(=R_0 + jX_0)$. Z_0, the impedance seen by the PA, is determined by the impedance of the matching network and the following circuits. Thus, the efficiency of the PA depends on C_S, X_{in}, R_{in}, and the design of the matching network.

B. Coupling Coils

As shown in Fig. 1(c), the coupling coils consist of the transmitting coil L_{tx} and the receiving coil L_{rx}. r_{tx} and r_{rx} are ESRs of L_{tx} and L_{rx}. C_{tx} and C_{rx} are the compensation capacitors. L_m is the mutual inductance

$$L_m = k\sqrt{L_{\text{tx}} L_{\text{rx}}} \tag{13}$$

where k is the mutual inductance coefficient, a parameter indicating the coil relative position. Based on the condition of $\omega L_{\text{tx}} = \frac{1}{\omega C_{\text{tx}}}$ (i.e., a resonating transmitting coil) and the equivalent circuit in Fig. 1(c), the resistance and reactance components of the input impedance of the coupling coils, Z_{in}

$(= R_{\text{in}} + jX_{\text{in}})$, can be expressed as

$$R_{\text{in}} = \frac{\omega^2 {L_m}^2 (R_{\text{rec}} + r_{\text{rx}})}{(R_{\text{rec}} + r_{\text{rx}})^2 + \left(X_{\text{rec}} + \omega L_{\text{rx}} - \frac{1}{\omega C_{\text{rx}}}\right)^2} + r_{\text{tx}} \quad (14)$$

$$X_{\text{in}} = -\frac{\omega^2 {L_m}^2 \left(X_{\text{rec}} + \omega L_{\text{rx}} - \frac{1}{\omega C_{\text{rx}}}\right)}{(R_{\text{rec}} + r_{\text{rx}})^2 + \left(X_{\text{rec}} + \omega L_{\text{rx}} - \frac{1}{\omega C_{\text{rx}}}\right)^2} \quad (15)$$

respectively. R_{rec} and X_{rec} are the resistance and reactance components of the input impedance of the Class *E* rectifier, Z_{rec}, (refer to the following subsection). For generality, in (14) and (15), the resonance of the receiving coil is not preassumed. For the coupling coils, the power losses occur on r_{tx} and r_{rx}. Thus, η_{coil} can be written as

$$\eta_{\text{coil}} = \frac{P_{\text{rec}}}{P_{Z_{\text{in}}}} = \frac{R_{\text{in}} - r_{\text{tx}}}{R_{\text{in}}} \cdot \frac{R_{\text{rec}}}{r_{\text{rx}} + R_{\text{rec}}}. \quad (16)$$

Substituting (13) and (14) into (16) gives the efficiency of the coupling coils

$$\eta_{\text{coil}} = \frac{R_{\text{rec}} \omega^2 k^2 L_{\text{tx}} L_{\text{rx}}}{\omega^2 k^2 L_{\text{tx}} L_{\text{rx}} (R_{\text{rec}} + r_{\text{rx}}) + r_{\text{tx}} b} \quad (17)$$

where

$$b = (R_{\text{rec}} + r_{\text{rx}})^2 + \left(X_{\text{rec}} + \omega L_{\text{rx}} - \frac{1}{\omega C_{\text{rx}}}\right)^2. \quad (18)$$

From (17) and (18), the efficiency of coupling coils is determined by k, C_{rx}, and Z_{rec}. As discussed in the following subsection, Z_{rec} depends on the final dc load, R_L, and the parallel capacitor of the Class *E* rectifier, C_r. Thus, the design parameters that influence the coil efficiency are C_{rx} and C_r. k and R_L are variables.

C. Class E Rectifier

As shown in Fig. 1(a), the Class *E* rectifier consists of a diode D_r, a parallel capacitor C_r, a filter capacitor C_o, and a filter inductor L_r. Here, R_L is the final dc load. In the rectifier, the parasitic capacitor of the diode is absorbed into the parallel capacitor C_r. r_{Lr} is the ESR of L_r and r_{D_r} is the on-resistance of the diode. L_r should be sufficiently large such that the current through it is constant and equal to the dc output current. A small output ripple voltage also requires a large C_o. The efficiency of the Class *E* current-driven half-wave rectifier has been derived in [25]. In order to facilitate the following discussions, the results are shown and explained as follows:

$$\eta_{\text{rec}} = \frac{P_o}{P_{\text{rec}}} = \frac{R_L}{R_L + r_{L_r} + \frac{c r_{D_r}}{\sin^2 \phi_{\text{rec}}}} \quad (19)$$

where

$$c = \frac{D}{2} + D\sin^2\phi_{\text{rec}} - \frac{1}{\pi}\sin\phi_{\text{rec}}\cos(\phi_{\text{rec}} - 2\pi D) + \frac{1}{8\pi}\sin(2\phi_{\text{rec}} - 4\pi D) + \frac{3}{8\pi}\sin 2\phi_{\text{rec}} \quad (20)$$

$$\phi_{\text{rec}} = \arctan\left[\frac{1 - \cos 2\pi D}{\sin(2\pi D) + 2\pi(1 - D)}\right]. \quad (21)$$

In the aforementioned equations ϕ_{rec} is the initial phase of the rectifier input current and c is an intermediate variable. D is the duty cycle of the diode, which can be implicitly expressed as

$$C_r = \frac{1 + \frac{[\sin(2\pi D) + 2\pi(1-D)]^2}{1 - \cos(2\pi D)} - 2\pi^2(1-D)^2 - \cos(2\pi D)}{2\pi\omega(R_L + r_{L_r} + r_{D_r})}. \quad (22)$$

Note that for generality, in the following derivations the value of D is not preassumed. From (19)–(22), it can be seen that the efficiency of the rectifier is determined by the dc load R_L and the parallel capacitor C_r. Thus, the design parameter of the rectifier is C_r, and R_L is a variable. For calculating the coupling coil efficiency, the input impedance of the rectifier, Z_{rec} $(= R_{\text{rec}} + jX_{\text{rec}})$, is also given as follows [25]:

$$R_{\text{rec}} = 2(R_L + r_{L_r})\sin^2\phi_{\text{rec}} + 2cr_{D_r} \quad (23)$$

$$X_{\text{rec}} = \frac{V_{m,X_{\text{rec}}}}{I_m} = -\frac{1}{\pi}\left[\frac{e+f}{\omega C_r} + r_{D_r}(g+h)\right] \quad (24)$$

where

$$e = \pi(1-D)\left[1 + 2\sin\phi_{\text{rec}}\sin(\phi_{\text{rec}} - 2\pi D)\right] \quad (25)$$

$$f = \sin(2\pi D) + \frac{1}{4}\left[\sin(2\phi_{\text{rec}} - 4\pi D) - \sin(2\phi_{\text{rec}})\right] \quad (26)$$

$$g = \frac{1}{2} - \frac{\cos(2\phi_{\text{rec}})}{4} - \frac{\cos(2\phi_{\text{rec}} - 4\pi D)}{4} \quad (27)$$

$$h = -\sin\phi_{\text{rec}}\sin(\phi_{\text{rec}} - 2\pi D) \quad (28)$$

$V_{m,X_{\text{rec}}}$ is the amplitude of the input voltage of the rectifier on X_{rec}, and I_m is the amplitude of the input current of the rectifier. The efficiency of the overall MHz WPT system, η_{sys}, can be obtained through the multiplication of (12), (17), and (19).

III. Robust Analysis and Design

In the existing design, the parameters of the Class E^2 dc–dc converter for MHz WPT are determined to satisfy the resonance of the two coupling coils and the zero-voltage-switching (ZVS) operation of the Class *E* PA under a single target operating condition. Meanwhile, in real applications, the variations of the mutual inductance coefficient k and the dc load R_L are usually inevitable. These variations will significantly affect the efficiency of the final WPT system. In the following subsections, the improvements under a varying operating condition are discussed. First, the robust analysis of the existing design of the Class E^2 dc–dc converter is given; then, the design of the PA matching network is improved for achieving a better robustness; finally, the design parameters are determined through a proposed design optimization procedure that aims at maintaining a high system efficiency over varying k and R_L.

A. Robust Analysis of Existing Design

As shown in Fig. 2, conventionally a series *LC* circuit is used as a matching network for the Class *E* PA [11], [13], [14], [25]. C_0 and L_0 are the series capacitor and inductor, and r_{L_0} is the ESR of L_0. Note that usually L_0 is considered to be a fixed

one and C_0 is the design parameter of the network. Based on the derivations in Section II, the system efficiency is determined by C_S, C_0, k, $C_{\rm rx}$, C_r, and R_L. As discussed previously, C_S, C_0, $C_{\rm rx}$, and C_r are the design parameters. k and R_L are the variables. In the existing design, the optimal design parameters of the Class E^2 dc–dc converter ($C_{S,\rm opt}$, $C_{0,\rm opt}$, $C_{rx,\rm opt}$, $C_{r,\rm opt}$) are calculated to achieve 1) 50% diode duty cycle of the rectifier; 2) resonance of the receiving coil; and 3) ZVS operation of the Class *E* PA [25]. For instance, under the constant parameters of the final experimental system, Table III in Section IV, the design parameters, ($C_{S,\rm opt}$, $C_{0,\rm opt}$, $C_{rx,\rm opt}$, $C_{r,\rm opt}$), are as follows at the target values of k (=0.203) and R_L (=30 Ω):

$$(100\,\mathrm{p}F, 1837\,\mathrm{p}F, 194\,\mathrm{p}F, 236\,\mathrm{p}F)\,. \tag{29}$$

Using the derived efficiencies in Section II, the system efficiencies under varying k and R_L are shown in Fig. 3(a) and (b), respectively. The results clearly show that the Class E^2 dc–dc converter can achieve a high efficiency at the target operating condition ($k = 0.203$, $R_L = 30\ \Omega$); however, its efficiency significantly decreases when k and R_L deviate from their target values, namely a poor robust performance. For a further investigation, the robustness indices, i.e., the greatest variations of component- and system-level efficiencies, are summarized in Table I under varying k (from 0.135 to 0.403) and R_L (from 15 Ω to 45 Ω). The so-called robustness index, α, is defined as follows:

$$\alpha_x = \max\left|\frac{\eta_x(k, R_L) - \eta_x(0.203, 30)}{\eta_x(0.203, 30)}\right| \tag{30}$$

where η with different subscripts (pa, coil, rec, and sys) represent the efficiencies of the PA, coupling coils, rectifier, and overall WPT system. This index is defined to quantify the range of the efficiency variation, i.e., the worst case, due to the uncertainties in k and R_L. Thus, "max" is used in the aforementioned equation.

As shown in Table I, the Class *E* PA demonstrates the worst robustness against the variations of k and R_L. Thus, in the following subsection, the classical matching network is modified that improves the robustness of the PA. In addition, as shown in the aforementioned derivations and discussions, there are complicated interactions among the components of the Class E^2 dc–dc converter. For example, the load of the PA, $Z_{\rm in}$, that determines the PA efficiency is influenced by the connected coupling coils, rectifier, and the dc load [refer to (14) and (15)]. For a robust operation of the Class E^2 dc–dc converter in real WPT applications, it is especially important to determine the design parameters in a system-level perspective, as discussed in Section III-C.

B. Improvement of Matching Network

From Fig. 2, it is straightforward to derive the impedance of the PA matching network, Z_0 ($= R_0 + jX_0$), in which

$$R_0 = R_{\rm in} + r_{L_0} \text{ and } X_0 = X_{\rm in} + \omega L_0 - \frac{1}{\omega C_0}. \tag{31}$$

It can be seen that R_0 and X_0 are proportional to $R_{\rm in}$ and $X_{\rm in}$, respectively. This explains the poor robustness of the Class *E* PA in Table I because the classical *LC* matching network cannot provide the required impedance compression when k and R_L vary. In order to improve the robustness of the PA, and thus, the overall WPT system, here the matching network is modified by adding a new shunt capacitor C_1, as shown in Fig. 4, i.e., a *T* matching network. The significance of adding this shunt capacitor is that it provides a capability to suppress the variation of Z_0, namely the impedance compression, as shown in (32) and (33)

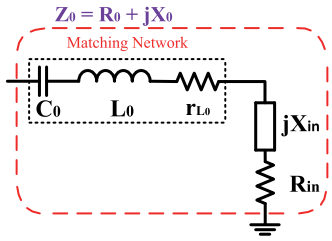

Fig. 2. *LC* matching network of the Class *E* PA.

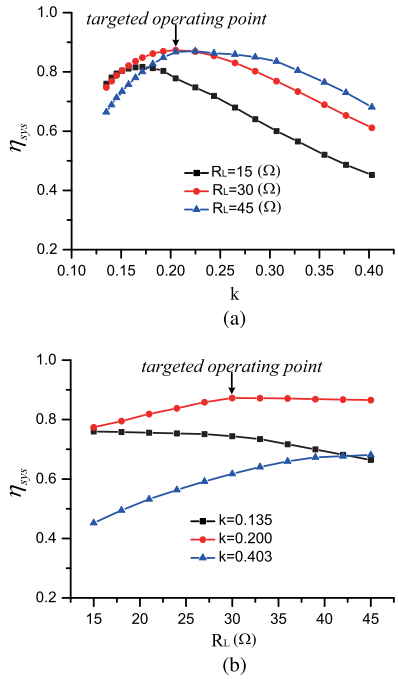

Fig. 3. System efficiency. (a) Under varying k. (b) Under varying R_L.

$$R_0 = r_{L_0} + \frac{R_{\rm in}}{\omega^2 {C_1}^2\left[\left(\frac{1}{\omega C_0} + \frac{1}{\omega C_1} - X_{\rm in}\right)^2 + {R_{\rm in}}^2\right]} \tag{32}$$

$$X_0 = \omega L_0 + \frac{\left(X_{in} - \frac{1}{\omega C_0}\right)\left(\frac{1}{\omega C_0} + \frac{1}{\omega C_1} - X_{in}\right) - {R_{\rm in}}^2}{\omega C_1\left[\left(\frac{1}{\omega C_0} + \frac{1}{\omega C_1} - X_{\rm in}\right)^2 + {R_{\rm in}}^2\right]} \tag{33}$$

where R_0 and X_0 are the equivalent resistance and reactance of the proposed *T* matching network. Note that adding the shunt

TABLE I
ROBUSTNESS INDICES

α_{pa}	α_{coil}	α_{rec}	α_{sys}
47.0%	5.3%	4.2%	47.6%

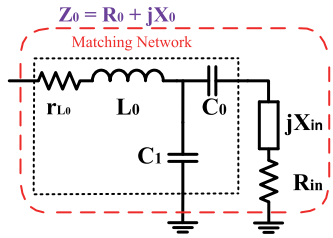

Fig. 4. T matching network of the Class E PA.

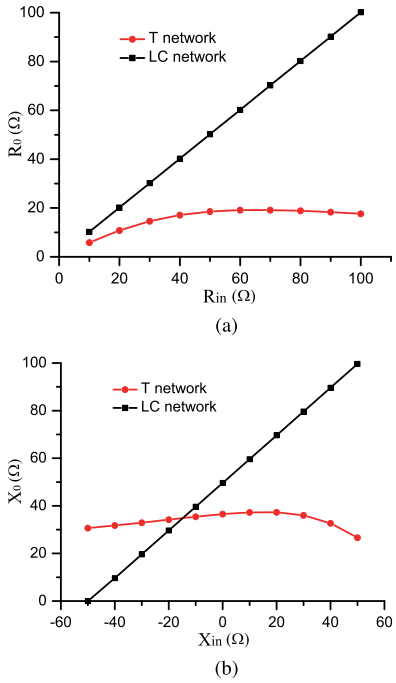

Fig. 5. R_0 and X_0 of the LC and T matching networks. (a) R_0 under a varying R_{in} and a fixed X_{in}. (b) X_0 under a varying X_{in} and a fixed R_{in}.

capacitor, C_1, basically does not increase the power loss on the PA due to the very small ESR of the capacitor. However, as discussed later, it requires a new design approach due to the increased complexity of the matching network.

It is interesting to note that with C_1 the relationship between Z_0 and Z_{in} could be significantly changed. Fig. 5 shows an example, in which the T matching network demonstrates a desired impedance compression capability. With properly designed C_0 and C_1, this advantage can improve the robustness the Class E PA against the variation of Z_{in}. In this example, C_0 in the classical LC matching network is 1837 pF [refer to (29)]; C_0 and C_1 in the T matching network are 1500 and 470 pF, respectively. The design of C_0 and C_1 in the T matching network is discussed in detail in the following subsection.

TABLE II
DEFINITIONS OF VECTORS

Vector	Components
$\mathbf{x}$	$[C_S,\ C_0,\ C_1,\ C_{\text{rx}},\ C_r]_{1\times5}$
$\mathbf{p_{var}}$	$[k,\ R_L]_{1\times2}$
$\mathbf{p_{var}^{nom}}$	$[k^{\text{nom}},\ R_L^{\text{nom}}]_{1\times2}$
$\mathbf{p_{var}^{lower}}$	$[k^{\min},\ R_L^{\min}]_{1\times2}$
$\mathbf{p_{var}^{upper}}$	$[k^{\max},\ R_L^{\max}]_{1\times2}$
$\mathbf{p_{con}}$	$[\omega,\ C_{\text{tx}},\ L_0,\ L_{\text{tx}},\ L_{\text{rx}},\ r_Q,\ r_{L_f},\ r_{L_0},\ r_{\text{tx}},\ r_{\text{rx}},\ r_{L_r},\ r_{D_r}]_{1\times12}$

C. Parameter Design Procedure

The components in the following parameter design are defined in vectors, as listed in Table II. As discussed previously, C_S, C_0, C_1, C_{rx}, and C_r are the five design parameters of the Class E^2 dc–dc converter using the T matching network (see Fig. 1(a) and Fig. 4), namely $\mathbf{x}$. The feasible range of $\mathbf{x}$ is defined as

$$\mathbf{x} \in \left(\mathbf{x^{lower}}, \mathbf{x^{upper}}\right) \tag{34}$$

where $\mathbf{x^{lower}}$ and $\mathbf{x^{upper}}$ are the lower and upper bounds of $\mathbf{x}$, respectively. The constant parameters in the Class E^2 dc–dc converter are represented by $\mathbf{p_{con}}$. In real applications, the variations in the mutual inductance coefficient k and the final dc load R_L are common. These two variables and their nominal values (i.e., a target operating condition) are defined as $\mathbf{p_{var}}$ and $\mathbf{p_{var}^{nom}}$, respectively. k^{nom} and R_L^{nom} are the nominal values of k and R_L. Again the variation range of $\mathbf{p_{var}}$ is defined as

$$\mathbf{p_{var}} \in \left(\mathbf{p_{var}^{lower}}, \mathbf{p_{var}^{upper}}\right) \tag{35}$$

where $\mathbf{p_{var}^{lower}}$ and $\mathbf{p_{var}^{upper}}$ are the lower and upper bounds of $\mathbf{p_{var}}$. $k^{\max}$, $k^{\min}$, $R_L^{\max}$, and $R_L^{\min}$ are the predefined maximum and minimum values of the two variables. The following parameter design procedure is developed considering the uncertainties in k and R_L.

From (1), (12), (17), (19), (32), and (33), the system efficiency can be expressed by a function of design parameters $\mathbf{x}$, constant parameters $\mathbf{p_{con}}$, and variables $\mathbf{p_{var}}$

$$\eta_{\text{sys}}(\mathbf{x}, \mathbf{p_{var}}) = f(\mathbf{x}, \mathbf{p_{con}}, \mathbf{p_{var}}). \tag{36}$$

Thus, the nominal system efficiency is

$$\eta_{\text{sys}}^{\text{nom}}(\mathbf{x}) = f(\mathbf{x}, \mathbf{p_{con}}, \mathbf{p_{var}^{nom}}). \tag{37}$$

Similarly, as defined in Section III-A, the index representing the robustness of the system efficiency against varying k and R_L is

$$\begin{aligned}\alpha_{\text{sys}}(\mathbf{x}) &= \max_{\mathbf{p_{var}}} \left| \frac{\eta_{\text{sys}}(\mathbf{x}, \mathbf{p_{var}}) - \eta_{\text{sys}}^{\text{nom}}(\mathbf{x})}{\eta_{\text{sys}}^{\text{nom}}(\mathbf{x})} \right| \\ &= \max_{\mathbf{p_{var}}} \left| \frac{f(\mathbf{x}, \mathbf{p_{con}}, \mathbf{p_{var}}) - f(\mathbf{x}, \mathbf{p_{con}}, \mathbf{p_{var}^{nom}})}{f(\mathbf{x}, \mathbf{p_{con}}, \mathbf{p_{var}^{nom}})} \right|. \end{aligned} \tag{38}$$

A smaller $\alpha_{\text{sys}}(\mathbf{x})$ means a higher robust performance requirement, and vice versa. Besides, a practical requirement is to lower the voltage stress on the diode in the Class E rectifier. It is known that generally a 50% duty cycle, D, of the rectifying diode minimizes the voltage stress. Note that the duty cycle of the switch,

TABLE III
CONSTANT PARAMETERS

ω	$C_{\rm tx}$	L_0	$L_{\rm tx}$	$L_{\rm rx}$	r_Q	r_{L_f}	r_{L_0}	$r_{\rm tx}$	$r_{\rm rx}$	r_{L_r}	r_{D_r}
6.78 MHz	165 pF	1.465 μH	3.34 μH	3.34 μH	0.23 Ω	0.2 Ω	0.4 Ω	0.7 Ω	0.7 Ω	0.2 Ω	1.4 Ω

Q, in the PA is fixed at 50%, which is a common practice when using the Class *E* PA [13], [29].

The final design optimization problem that determines $\mathbf{x}$ is formulated as follows:

$$\max_{\mathbf{x}} \quad \eta_{\rm sys}^{\rm nom}(\mathbf{x}) \tag{39}$$

$$s.t. \quad \alpha_{\rm sys}(\mathbf{x}) \le \alpha_{\rm sys}^{\max} \tag{40}$$

$$\max_{\mathbf{p_{var}}} |D(\mathbf{x}, \mathbf{p_{con}}, \mathbf{p_{var}}) - 0.5| \le \beta_D^{\max}. \tag{41}$$

The requirements on the robustness and a proper duty cycle (around 50%) of the rectifying diode are represented as two constraints, (40) and (41), in the optimization problem. Note that $\alpha_{\rm sys}^{\max}$ and $\beta_D^{\max}$ are the maximum permissible values, i.e., the worst cases. They limit deviations of the system efficiency and the duty cycle of the rectifying diode from their nominal values, $\eta_{\rm sys}^{\rm nom}(\mathbf{x})$ and D (=50%), respectively. These two maximum permissible values should be specified based on the performance and design requirements of a target application. The duty cycle of the rectifying diode, $D(\mathbf{x}, \mathbf{p_{con}}, \mathbf{p_{var}})$ in (41), is solved using (22). Note that (41) is a constraint to lower the voltage stress on the rectifying diode, i.e., a duty cycle, D, around 50%. The purpose of the design procedure is to find an optimal set of the design parameters, $\mathbf{x_{opt}}$, that 1) meets the two constraints on the robustness and the duty cycle of the diode in the rectifier and 2) leads to the highest achievable system efficiency under the two constraints and the nominal k and R_L. Given the nature of the optimization problem in (39)–(41), it is appropriate to apply genetic algorithm (GA), a popular population-based heuristic approach, to find a global or at least near-to-global optimal solution [30], [31]. Candidate $\mathbf{x}$'s are generated and checked for the constraints violation. Final candidate $\mathbf{x}$'s are the solutions satisfying the two constraints, namely (40) and (41). The optimal $\mathbf{x_{opt}}$ is one of the final candidates that corresponds to the highest achievable $\eta_{\rm sys}^{\rm nom}(\mathbf{x})$ and meets the constraints at the same time.

IV. EXPERIMENTAL VERIFICATION

As shown in Fig. 6, an example Class E^2 dc–dc converter working at 6.78 MHz is built up for verification purposes. The WPT system has the same configuration as the one in Fig. 1. Note that the *T* matching network is implemented by adding an additional shunt capacitor, C_1, in the PA circuit (refer to Fig. 4).

In the experiments, the input dc voltage of the PA, $V_{\rm pa}$, is fixed at 22 V to achieve 10-W dc input power at the target operating condition ($k = 0.203$ and $R_L = 30\ \Omega$). Table III lists the values of the constant parameters, $\mathbf{p_{con}}$. The inductances and ESRs of the coupling coils, $L_{\rm tx}$, $L_{\rm rx}$, $r_{\rm tx}$, and $r_{\rm rx}$, are measured by a vector network analyzer. The variation of the mutual inductance coefficient, k, is realized by adjusting the distance between the coupling coils, d (see Fig. 6). Table IV shows the relationship between k and d. The parameter k is also measured by the vector network analyzer. It varies from 0.403 to 0.135 when d is adjusted from 15 to 45 mm. Here, the nominal d and dc load, $d^{\rm nom}$ and $R_L^{\rm nom}$, are specified as 30 mm and 30 Ω, respectively. From Table IV, the corresponding $\mathbf{p_{var}^{nom}}$, i.e., the nominal values of the two variables (k and R_L), is (0.203, 30). In the following experiments, the variation ranges of d and R_L around their nominal values are both $\pm 50\%$. From Table IV, correspondingly k ranges from 66.5% to 198.5% of its nominal value, $k = 0.203$. Note that without coil misalignment d and k has a one-to-one relationship and k is determined by a specific d.

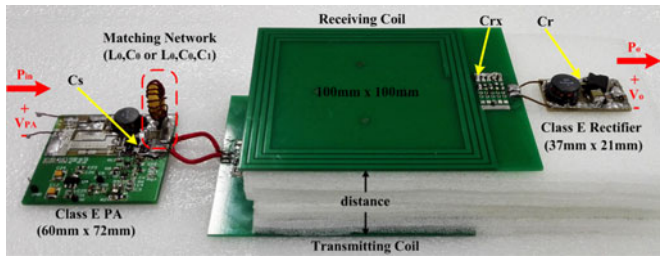

Fig. 6. Example 6.78-MHz Class E^2 dc–dc converter for WPT.

TABLE IV
MUTUAL INDUCTANCE COEFFICIENT VERSUS COIL DISTANCE

d (mm)	15	20	25	30	35	40	45
k	0.403	0.328	0.265	0.203	0.172	0.151	0.135

Here, the feasible ranges of the design parameters, $\mathbf{x} = [C_S, C_0, C_1, C_{\rm rx}, C_r]$, are given as

$$\mathbf{x^{lower}} = [100\ \text{pF}, 100\ \text{pF}, 100\ \text{pF}, 100\ \text{pF}, 100\ \text{pF}]$$
$$\mathbf{x^{upper}} = [2000\ \text{pF}, 2000\ \text{pF}, 2000\ \text{pF}, 2000\ \text{pF}, 2000\ \text{pF}]. \tag{42}$$

The aforementioned ranges are defined referring to the result of the existing design, (29). This is because (29) is an optimized design that indicates the required impedance characteristics around the target operation condition, i.e., k (=0.203) and R_L (=30 Ω). In order to have a proper voltage stress on the diode of the Class *E* rectifier, $\beta_D^{\max}$ in the constraint on the diode duty cycle, (41), is taken as 0.1. Thus, the permissible variation of the duty cycle of the rectifying diode is between 0.4 and 0.6 when d and R_L vary between $\pm 50\%$ of their nominal values. For the selection of $\alpha_{\rm sys}^{\max}$ in the constraint (40), there is a tradeoff relationship between the system performance, i.e., the efficiency, and the required robustness. Here, $\alpha_{\rm sys}^{\max}$ is chosen to be 0.2. Note that a small $\alpha_{\rm sys}^{\max}$,

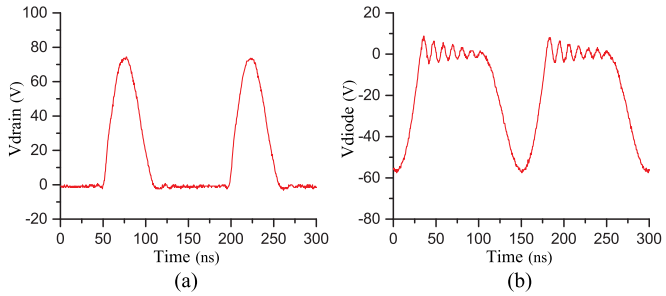

Fig. 7. Experimental waveforms of the Class E^2 dc–dc converter. (a) Drain–source voltage of the switch Q in the Class E PA. (b) Voltage of the diode D_r in the Class E rectifier.

i.e., a requirement of high robustness, may lead to poor system efficiency or no solution to the optimization problem, while a high $\alpha_{\text{sys}}^{\max}$ sacrifices the robustness against the variations in d (i.e., k) and R_L. Again the two maximum permissible values in the constraints should be specified based on the requirements from a real application.

In the experiments, a MOSFET SUD06N10 and a silicon carbide diode STPSC406 work as the switch Q and the rectifying diode D_r of the Class E PA and rectifier, respectively (refer to Fig. 1). Based on the datasheets, the parasitic capacitances of the switch and diode are 50 and 30 pF. The calculated final C_S and C_r include the two parasitic capacitances, respectively. Following the design procedure developed in Section III-C, the optimal design parameters, $\mathbf{x_{opt}}$, are

$$\mathbf{x_{opt}} = [150 \text{ pF}, 1500 \text{ pF}, 470 \text{ pF}, 180 \text{ pF}, 300 \text{ pF}]. \quad (43)$$

It is found that the solutions of the GA-based optimization in the robust design are similar. The optimal parameters in (43) are finalized considering the capacitances of the commercially available products. Note that the results of the existing design are summarized in (29). For reference purposes, the two key waveforms of the Class E^2 dc–dc converter (the drain–source voltage of the switch Q in the PA and the voltage of the diode D_r in the rectifier) are shown in Fig. 7. The performances of using the two designs are compared in experiments when d and R_L vary ($\pm 50\%$).

Fig. 8 shows the experimental (exp.) and calculated (cal.) results of the system efficiency versus the mutual inductance coefficient, k, in which k varies from 0.135 to 0.403. d_{min}, d_{nom}, and $d_{\max}$ in the figure are 15, 30, and 45 mm, respectively. As shown in Fig. 8(b), the Class E^2 dc–dc converters designed by the robust and existing approaches both achieve a high system efficiency under the nominal k (=0.203) and R_L (=30 Ω). Meanwhile, when k and R_L deviate from their nominal values, the existing design shows an obvious poorer robustness, i.e., a bigger drop of the system efficiency, than that of the robust design. The calculated results use the efficiencies analytically derived in Section II. The good matching between the experimental and calculated results well verifies the correctness of the equations of the efficiencies. The slight differences between the experimental and calculated efficiencies are mainly caused by the modeling error in Z_{in}, the load of the Class E PA (see Fig. 1). Due to the nonlinearity existing between the PA's efficiency and its load, the calculated efficiencies may be either slightly higher or lower than the experimental efficiencies. The system efficiency versus the dc load, R_L, is also shown in Fig. 9. Again similar results can be observed. Under varying R_L and k (i.e., d), the Class E^2 dc–dc converter whose parameters are determined through the robust design demonstrates obviously better robustness than the converter designed using the existing approach. For reference purposes, the robust indices in the experiments are listed in Table V that quantify the improvements using the proposed robust design [refer to (30)]. As shown in Figs. 8 and 9, and Table V, the proposed robust design enables the load sensitive Class E PA to work close to its ZVS operation over the wide ranges of the mutual inductance coefficient (i.e., the coil relative position) and the final dc load. This explains the high system efficiencies achieved through the robust design.

Fig. 10 gives the experimental and calculated duty cycle, D, of the diode in the rectifier versus the dc load, R_L. Note that D is irrelevant to k (i.e., d), as shown in (22). D is well controlled to be within 0.4 and 0.6, which satisfies the constraint (41) on reducing the voltage stress of the rectifying diode. Again the good match between the experimental and calculated results validates the previous analytical derivations, particularly (22).

Fig. 11 shows the output power of the Class E^2 dc–dc converter, P_o, using the two design approaches, the robust and existing ones. P_o is the power received by the final dc load, R_L [see Fig. 1(a)]. As same as in Figs. 8 and 9, the following comparisons are under a same dc input voltage of the Class E PA, V_{pa} (=22 V). It is interesting to note that although the robust design is originally developed to maximize the achievable system efficiency, the design also enables higher output power than that of the existing design under the most k's (i.e., d's) and R_L's. Thus, it is possible to design a MHz WPT system that achieves the same output power with a lower dc input voltage. The requirement of a lower dc input voltage is usually advantageous for real implementations. As discussed previously, the Class E PA can only efficiently work within a narrow range of the load [14]. With the newly added shunt capacitor, C_1, the T matching network of the PA performs the impedance compression that suppresses the variation of the load seen by the PA, Z_0 [refer to Figs. 1(b) and 5]. This leads to a higher input power of the coils, $P_{Z_{in}}$, and thus, a higher output power, P_o.

For reference purposes, the experimental efficiencies under the constant dc input voltage V_{pa} (=22 V) and the constant output power P_o (=10 W), respectively, are shown in Fig. 12, taking the cases of R_L = 30 Ω and k = 0.203 as examples. The constant output power is achieved by tuning V_{pa} properly. In the robust design V_{pa}'s for $d^{\max}$, d^{nom}, and $d^{\min}$ are 36.9, 24.1, and 16.2 V, respectively, while in the existing design the voltages are 36.7, 32.4, and 39.7 V, respectively. It can be seen that the efficiencies under both the constant dc input voltage and the constant output power are almost identical. As aforementioned discussion, the comparisons under a constant dc input voltage help to better explain another potential advantage of the proposed robust design—a lower dc input voltage when working with the same output power. As discussed in the introduction, this paper aims for application in electronic devices (e.g.,

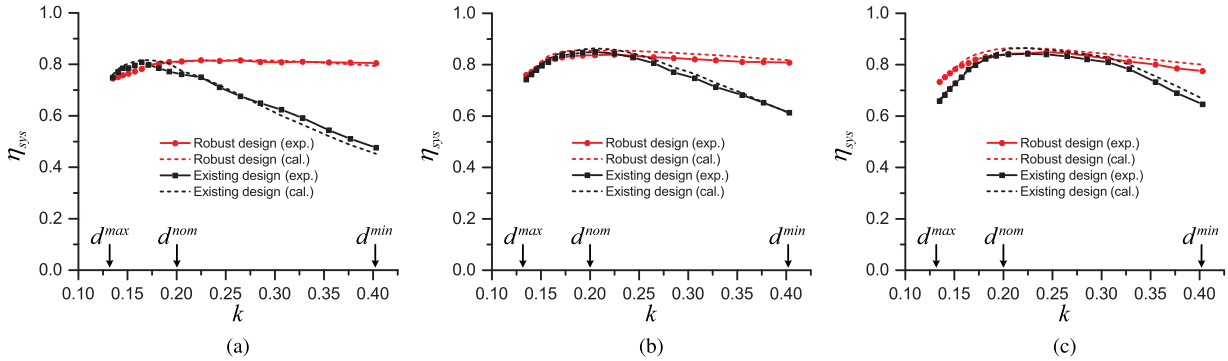

Fig. 8. System efficiency, η_{sys}, versus mutual inductance coefficient, k. (a) Results when $R_L = 15\ \Omega$. (b) Results when nominal $R_L = 30\ \Omega$. (c) Results when $R_L = 45\ \Omega$.

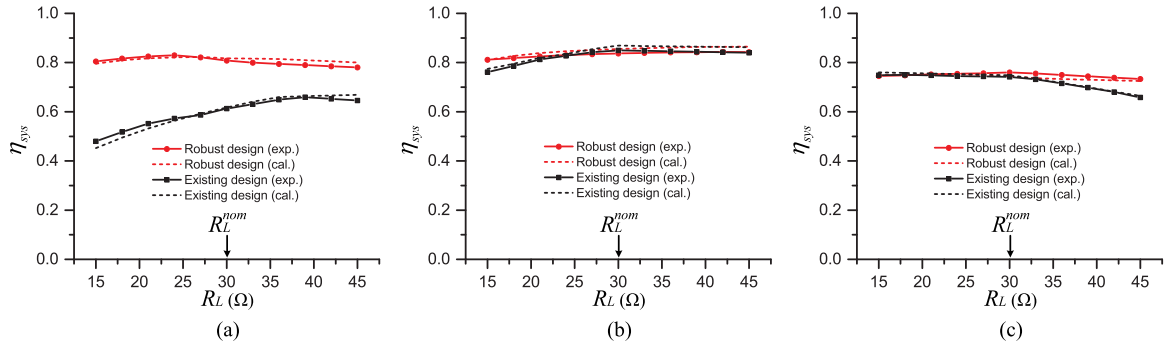

Fig. 9. System efficiency, η_{sys}, versus final dc load, R_L. (a) Results when $k = 0.403$ ($d = 15$ mm). (b) Results when nominal $k = 0.203$ ($d = 30$ mm). (c) Results when $k = 0.135$ ($d = 45$ mm).

TABLE V
ROBUSTNESS INDICES IN EXPERIMENTS

	α_{pa}	α_{coil}	α_{rec}	α_{sys}
Robust Design	11.1%	3.3%	3.1%	12.4%
Existing Design	43.3%	5.8%	4.2%	44.1%

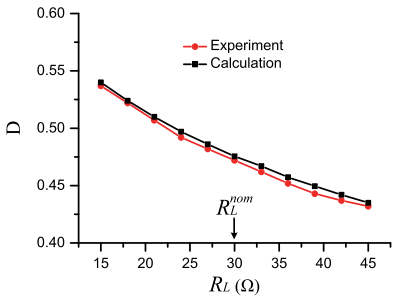

Fig. 10. Experimental and calculated duty cycle, D, of the diode of the Class E rectifier using the robust design.

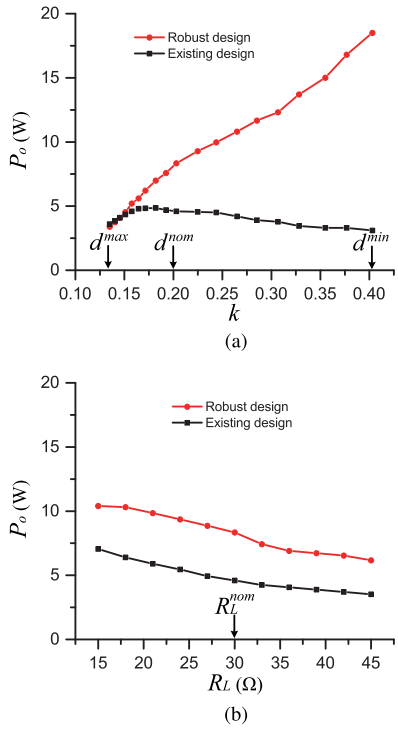

Fig. 11. Experimental system output power. (a) Results with nominal R_L (=30 Ω). (b) Results with nominal k (=0.203)/d (=30 mm).

cellphones, laptop computer, tablets, medical implant devices, etc.), whose power levels are suitable for WPT systems working in the MHz frequency range.

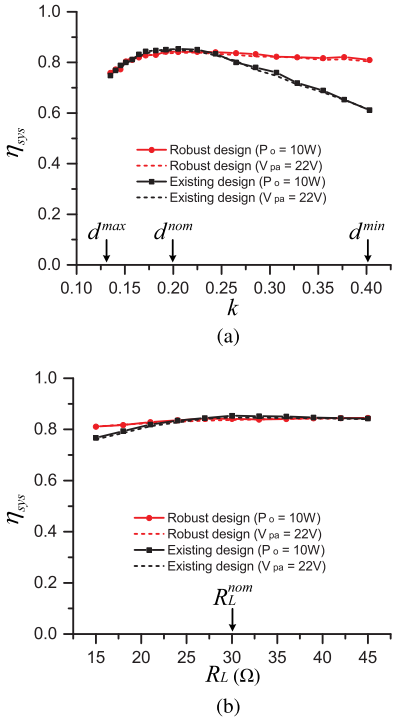

Fig. 12. Experimental comparisons of the system efficiencies when the output power is constant, P_o (=10 W). (a) Results with nominal R_L (=30 Ω). (b) Results with nominal k (=0.203) / d (=30 mm).

V. Conclusion

This paper discusses a robust design of a Class E^2 dc–dc converter for MHz WPT. The component (rectifier, coupling coil, and PA) and system efficiencies are analytically derived in a general form, where the resonance of the receiving coil and the duty cycle of the rectifying diode are not preassumed. The initial four design parameters are then determined based on the results of the derivations. The following analysis shows that the existing design has a poor robustness against the variations in the mutual inductance coefficient and the final load. In order to improve the robustness, the classical matching network of the PA is modified by adding a new shunt capacitor. This provides the matching network the required impedance compression capability. The capacitance of the shunt capacitor is added as a new design parameter, i.e., five design parameters in total. Then, the parameter design procedure is developed, in which the requirements on the robustness and a proper voltage stress on the rectifying diode are represented through the two constraints. Both the experimental and calculated results show that the robustness of the efficiency of the example 6.78-MHz Class E^2 dc–dc converter is obviously improved through the proposed robust design approach. For example, the experiments show that the range of variation of the system efficiency is narrowed from 47.5%–85.0% to 73.3%–83.7%. A good matching between the experimental and calculated results also validates the analytical derivations. The methodology developed in paper, i.e., the derivations of efficiencies, improvement of PA matching network, and robust parameter design, is a general one that can be extended to other Class E^2 dc–dc converters with different topologies, i.e., various combinations of coupling coils (series–series, parallel–series, series–parallel, and parallel–parallel) and the Class E rectifier (current- and voltage-driven, half- and full wave).

References

[1] A. P. Sample, B. H. Waters, S. T. Wisdom, and J. R. Smith, "Enabling seamless wireless power delivery in dynamic environments," *Proc. IEEE*, vol. 101, no. 6, pp. 1343–1358, Apr. 2013.

[2] S. Hui, W. Zhong, and C. Lee, "A critical review of recent progress in mid-range wireless power transfer," *IEEE Trans. Power Electron.*, vol. 29, no. 9, pp. 4500–4511, Sep. 2014.

[3] N. Keeling *et al.*, "A unity-power-factor IPT pickup for high-power applications," *IEEE Trans. Ind. Electron.*, vol. 57, no. 2, pp. 744–751, Feb. 2010.

[4] H. Li, K. W. Jie Li, W. Chen, and X. Yang, "A maximum efficiency point tracking control scheme for wireless power transfer systems using magnetic resonant coupling," *IEEE Trans. Power Electron.*, vol. 30, no. 7, pp. 3998–4008, Jul. 2015.

[5] W. Zhong and S. Hui, "Maximum energy efficiency tracking for wireless power transfer systems," *IEEE Trans. Power Electron.*, vol. 30, no. 7, pp. 4025–4034, Jul. 2015.

[6] A. Kurs, A. Karalis, R. Moffatt, J. D. Joannopoulos, P. Fisher, and M. Soljačić, "Wireless power transfer via strongly coupled magnetic resonances," *Science*, vol. 317, no. 5834, pp. 83–86, Jul. 2007.

[7] M. Pinuela, D. C. Yates, S. Lucyszyn, and P. D. Mitcheson, "Maximizing DC-to-load efficiency for inductive power transfer," *IEEE Trans. Power Electron.*, vol. 28, no. 5, pp. 2437–2447, May 2013.

[8] W. Zhong, C. Zhang, X. Liu, and S. Hui, "A methodology for making a three-coil wireless power transfer system more energy efficient than a two-coil counterpart for extended transfer distance," *IEEE Trans. Power Electron.*, vol. 30, no. 2, pp. 933–942, Feb. 2015.

[9] M. Fu, T. Zhang, C. Ma, and X. Zhu, "Efficiency and optimal loads analysis for multiple-receiver wireless power transfer systems," *IEEE Trans. Microw. Theory Techn.*, vol. 63, no. 3, pp. 801–812, Mar. 2015.

[10] N. Sokal and A. Sokal, "Class E-A new class of high-efficiency tuned single-ended switching power amplifiers," *IEEE J. Solid-State Circuits*, vol. 10, no. 3, pp. 168–176, Jun. 1975.

[11] W. Chen, R. Chinga, S. Yoshida, J. Lin, C. Chen, and W. Lo, "A 25.6 W 13.56 MHz wireless power transfer system with a 94% efficiency GaN class-E power amplifier," in *Proc. IEEE MTT-S Int. Microw. Symp.*, Montreal, Canada, Jun. 2012, pp. 1–2.

[12] S. Aldhaher, P.-K. Luk, A. Bati, and J. Whidborne, "Wireless power transfer using Class E inverter with saturable DC-feed inductor," *IEEE Trans. Ind. Appl.*, vol. 50, no. 4, pp. 2710–2718, Jul. 2014.

[13] S. Aldhaher, P.-K. Luk, and J. F. Whidborne, "Electronic tuning of misaligned coils in wireless power transfer systems," *IEEE Trans. Power Electron.*, vol. 29, no. 11, pp. 5975–5982, Nov. 2014.

[14] S. Liu, M. Liu, M. Fu, C. Ma, and X. Zhu, "A high-efficiency Class-E power amplifier with wide-range load in WPT systems," in *Proc. IEEE Wireless Power Transfer Conf.*, Boulder, CO, USA, May 2015, pp. 1–3.

[15] W. Nitz, W. Bowman, F. Dickens, F. Magalhaes, W. Strauss, W. Suiter, and N. Ziesse, "A new family of resonant rectifier circuits for high frequency DC-DC converter applications," in *Proc. IEEE Appl. Power Electron. Conf. Exp.*, New Orleans, LA, USA, Feb. 1988.

[16] M. Kazimierczuk and J. Jozwik, "Class-E zero-voltage-switching and zero-current-switching rectifiers," *IEEE Trans. Circuits Syst.*, vol. 37, no. 3, pp. 436–444, Mar. 1990.

[17] A. Ivascu, M. Kazimierczuk, and S. Birca-Galateanu, "Class E resonant low dv/dt rectifier," *IEEE Trans. Circuits Syst. I, Fundam. Theory Appl.*, vol. 39, no. 8, pp. 604–613, Aug. 1992.

[18] M. Kazimierczuk and W. Szaraniec, "Analysis of a Class E rectifier with a series capacitor," *Proc. IEE*, vol. 139, no. 3, pp. 269–276, Jun. 1992.

[19] M. Kazimierczuk, "Class E low $\mathrm{dv_d/dt}$ rectifier," *IEEE Trans. Power Electron.*, vol. 136, no. 6, pp. 257–262, Nov. 1989.

[20] A. Reatti, M. Kazimierczuk, and R. Redl, "Class E full-wave low dv/dt rectifier," *IEEE Trans. Circuits Syst. I, Fundam. Theory Appl.*, vol. 40, no. 2, pp. 73–85, Feb. 1993.

[21] Y. Minami and H. Koizumi, "Analysis of Class DE current driven low di/dt rectifier," *IEEE Trans. Power Electron.*, vol. 30, no. 12, pp. 6804–6816, Dec. 2015.

[22] S. Aldhaher, P.-K. Luk, K. El Khamlichi Drissi, and J. Whidborne, "High-input-voltage high-frequency Class E rectifiers for resonant inductive links," *IEEE Trans. Power Electron.*, vol. 30, no. 3, pp. 1328–1335, Mar. 2015.

[23] P.-K. Luk, S. Aldhaher, W. Fei, and J. Whidborne, "State-space modeling of a Class E^2 converter for inductive links," *IEEE Trans. Power Electron.*, vol. 30, no. 6, pp. 3242–3251, Jun. 2015.

[24] G. Kkelis, J. Lawson, D. Yates, M. Pinuela, and P. Mitcheson, "Integration of a Class-E low dv/dt rectifier in a wireless power transfer system," in *Proc. IEEE Wireless Power Transfer Conf.*, Jeju, Korea, May 2014, pp. 72–75.

[25] M. Liu, M. Fu, and C. Ma, "Parameter design for a 6.78-MHz wireless power transfer system based on analytical derivation of class e current-driven rectifier," *IEEE Trans. Power Electron.*, vol. 31, no. 6, pp. 4280–4291, Jun. 2016.

[26] C.-S. Wang, G. A. Covic, and O. H. Stielau, "Investigating an LCL load resonant inverter for inductive power transfer applications," *IEEE Trans. Power Electron.*, vol. 19, no. 4, pp. 995–1002, Jul. 2004.

[27] M. Borage, S. Tiwari, and S. Kotaiah, "Analysis and design of an LCL-T resonant converter as a constant-current power supply," *IEEE Trans. Ind. Electron.*, vol. 52, no. 6, pp. 1547–1554, Dec. 2005.

[28] M. Albulet, *RF Power Amplifiers*. Raleigh, NC, USA: SciTech Publishing, 2001.

[29] T. Suetsugu and M. Kazimierczuk, "Analysis and design of Class E amplifier with shunt capacitance composed of nonlinear and linear capacitances," *IEEE Trans. Circuits Syst.*, vol. 51, no. 7, pp. 1261–1268, Jul. 2004.

[30] M. Li, S. Azarm, and A. Boyars, "A new deterministic approach using sensitivity region measures for multi-objective robust and feasibility robust design optimization," *J. Mech. Des.*, vol. 128, no. 4, pp. 874–883, Jul. 2006.

[31] M. J. Neath, A. K. Swain, U. K. Madawala, and D. J. Thrimawithana, "An optimal PID controller for a bidirectional inductive power transfer system using multiobjective genetic algorithm," *IEEE Trans. on Power Electron.*, vol. 29, no. 3, pp. 1523–1531, Mar. 2014.

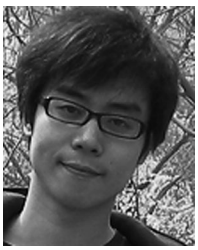

Ming Liu (S'15) received the B.S. degree from SiChuan University, Sichuan, China, in 2007, and the M.S. degree from the University of Science and Technology Beijing, Beijing, China, in 2011, both in mechatronic engineering. He is currently working toward the Ph.D. degree in electrical and computer engineering, University of Michigan-Shanghai Jiao Tong University Joint Institute, Shanghai Jiao Tong University, Shanghai, China.

His researches include design and optimization of megahertz wireless power transfer systems and high-frequency power electronic circuits.

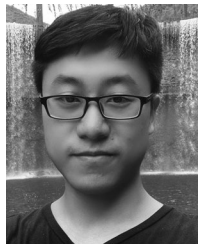

Yue Qiao received the B.S., M.S., and Ph.D. degrees in electrical and computer engineering from the University of Michigan-Shanghai Jiao Tong University Joint Institute, Shanghai Jiao Tong University, Shanghai, China, in 2010, 2013, and 2016, respectively.

He is currently a Software Engineer in GE AVIC Civil Avionics Systems Company Limited, Shanghai, China. His research interests include optimization algorithms, theory and application of motion control, and mechatronics.

Shuangke Liu (S'15) received the B.S. degree in electronics information engineering from Xidian University, Xi'an, China, in 2013. She is currently working toward the Ph.D. degree in electrical and computer engineering, University of Michigan-Shanghai Jiao Tong University Joint Institute, Shanghai Jiao Tong University, Shanghai, China.

Her research interests include megahertz wireless power transfer systems and RF/microwave circuits.

Chengbin Ma (M'05) received the B.S. (Hons.) degree in industrial automation from the East China University of Science and Technology, Shanghai, China, in 1997, and the M.S. and Ph.D. degrees both in electrical engineering from the University of Tokyo, Tokyo, Japan, in 2001 and 2004, respectively.

He is currently an Assistant Professor of electrical and computer engineering with the University of Michigan-Shanghai Jiao Tong University Joint Institute, Shanghai Jiao Tong University, Shanghai, China. He is also with a joint faculty appointment in the School of Mechanical Engineering, Shanghai Jiao Tong University. Between 2006 and 2008, he was a Postdoctoral Fellow with the Department of Mechanical and Aeronautical Engineering, University of California Davis, Davis, CA, USA. From 2004 to 2006, he was an R&D Researcher with Servo Laboratory, Fanuc Limited, Yamanashi Prefecure, Japan. His research interests include wireless power transfer, networked hybrid energy systems, and mechatronic control.